Lagged atmospheric circulation response in the Black Sea region to Greenland Interstadial 10

Markus Czymzik[a,1], Norbert R. Nowaczyk[b], Olaf Dellwig[a], Antje Wegwerth[a], Raimund Muscheler[c], Marcus Christl[d], and Helge W. Arz[a]

[a]Marine Geology, Leibniz Institute for Baltic Sea Research Warnemünde, 18119 Rostock, Germany; [b]Climate Dynamics and Landscape Evolution, Helmholtz Centre Potsdam German Research Centre for Geosciences, 14473 Potsdam, Germany; [c]Department of Geology, Lund University, 22362 Lund, Sweden; and [d]Laboratory of Ion Beam Physics, Eidgenössische Technische Hochschule Zurich, 8093 Zurich, Switzerland

Edited by Dominik Fleitmann, University of Reading, Reading, UK, and accepted by Editorial Board Member Jean Jouzel October 5, 2020 (received for review March 24, 2020)

Northern Hemispheric high-latitude climate variations during the last glacial are expected to propagate globally in a complex way. Investigating the evolution of these variations requires a precise synchronization of the considered environmental archives. Aligning the globally common production rate variations of the cosmogenic radionuclide ^{10}Be in different archives provides a tool for such synchronizations. Here, we present a ^{10}Be record at <40-y resolution along with subdecadal proxy records from one Black Sea sediment core around Greenland Interstadial 10 (GI-10) ∼41 ka BP and the Laschamp geomagnetic excursion. We synchronized our ^{10}Be record to that from Greenland ice cores based on its globally common production rate variations. The synchronized environmental proxy records reveal a bipartite climate response in the Black Sea region at the onset of GI-10. First, in phase with Greenland warming, reduced sedimentary coastal ice rafted detritus contents indicate less severe winters. Second, and with a lag of 190 (± 44) y, an increase in the detrital K/Ti ratio and authigenic Ca precipitation point to enhanced regional precipitation and warmer lake surface temperatures. We explain the lagged climatic response by a shift in the dominant mode of atmospheric circulation, likely connected with a time-transgressive adjustment of the regional thermal ocean interior to interstadial conditions.

cosmogenic radionuclides | archive synchronization | Black Sea sediments | climate | phase relationship

Northern Hemisphere climate during the last glacial cycle (Marine Isotope Stages 2 to 4) was primarily characterized by distinct switches between stadial and interstadial conditions during so-called Dansgaard–Oeschger or Greenland Interstadial (GI) events (1, 2). Abrupt interstadial warming was most pronounced in the high latitudes, occurred within decades or less, and lasted from a few hundred to some thousand years. Cold stadials were characterized by a more stable climate, but comparable ranges of durations (1, 2). Most-often proposed triggers of GIs are the glacial reinvigoration of the Atlantic Meridional Overturning Circulation due to fresh water perturbations and "spontaneous" reductions in sea ice cover in the Nordic Seas associated with thermohaline convective instability causing the release of accumulated oceanic heat to the atmosphere (2–5). Subsequently, these major shifts in high-latitude climate are expected to evolve globally in a complex manner, resulting in a range of region-specific expressions with possible lags in timing, and varying lengths, shapes, or amplitudes (2, 6). Proposed causal links for this behavior are interactions between fast atmospheric as well as slower cryospheric and oceanic processes (2, 6–8). However, the detailed progression of these abrupt climate shifts as well as their driving mechanisms are still poorly understood.

Main limitations for a better understanding of progressing GI climate variations are cross-dating uncertainties between individual environmental archives and the common practice of climate wiggle matching, impeding the detection of possible climate diachrony from the start (9–11). A way to circumvent these limitations is a climate-independent synchronization of the considered archives. In addition to tephra layers and atmospheric trace gases, cosmogenic radionuclides like ^{10}Be can serve as climate-independent synchronization tools for natural archives (12, 13). The ^{10}Be is produced in Earth's upper atmosphere through cascades of nuclear reactions during collisions of galactic cosmic rays with N and O atoms (14). While the galactic cosmic ray flux outside the heliosphere is assumed to be stable over the last million years, the flux arriving at Earth is modulated through varying heliomagnetic and geomagnetic shielding (14, 15). Therefore, during periods of reduced (higher) solar activity and geomagnetic field strength, more (less) ^{10}Be is produced. After its production, ^{10}Be is globally mixed during its about 1-y stratospheric residence time and deposited on Earth's surface through wet and dry deposition (16). Detecting and aligning the external ^{10}Be production signal in environmental archives like sediments and ice allows us to synchronize these records via curve fitting methods (12, 13). Prerequisite is the assessment and removal of possible nonproduction variability introduced into ^{10}Be records mainly by varying meteorological conditions during its about 1-mo tropospheric residence time and catchment processes (16–18).

Significance

Abrupt climate shifts in the Northern Hemisphere high latitudes during the last glacial propagate globally in a complex manner. Our understanding of this propagation is poor mainly due to cross-dating uncertainties between individual paleoclimate archives. We apply a record of the globally common ^{10}Be production rate variations to synchronize the Black Sea sediment record to central Greenland ice cores and investigate the hemispheric propagation of Greenland Interstadial 10, with minimized uncertainties in the relative timing. Our results suggest a bipartite climate response in the Black Sea region to the onset of the Greenland Interstadial, characterized by an in-phase decrease in winter severity and lagged shift in atmospheric circulation, explained by a time-transgressive thermal adjustment of the regional ocean interior.

Author contributions: M. Czymzik designed research; M. Czymzik performed research; M. Czymzik contributed new reagents/analytic tools; M. Czymzik, O.D., M. Christl, and H.W.A. analyzed data; and M. Czymzik, N.R.N., O.D., A.W., R.M., M. Christl, and H.W.A. wrote the paper.

The authors declare no competing interest.

This article is a PNAS Direct Submission. D.F. is a guest editor invited by the Editorial Board.

[1]To whom correspondence may be addressed. Email: markus.czymzik@io-warnemuende.de.

This article contains supporting information online at https://www.pnas.org/lookup/suppl/doi:10.1073/pnas.2005520117/-/DCSupplemental.

First published November 2, 2020.

Existing studies on the evolution of major Northern Hemispheric climate switches based on synchronized environmental records are noncomprehensive. A case study synchronizing two lake sediment records from central Norway and western Germany, using the Icelandic Vedde Ash isochrone (~12.15 ka BP), suggests that a major shift toward windier conditions within the Younger Dryas cold period occurred locally abruptly, but time-transgressively with an offset of ~120 y between both locations (6). Since the recorded proxy shifts are located close to the tephra layer in each archive, the chronological uncertainty connected with this result is likely low. Another study of central Greenland ice cores and tropical speleothems synchronized based on cosmogenic radionuclides suggests that climate shifts during the last glacial connected with GIs occur simultaneous, within errors of ± 189 y (19). Further studies applying synchronized paleoclimate records are required to understand the progression of high-latitude climate shifts throughout the Northern Hemisphere at down to multidecadal scales.

Synchronizing the Black Sea Sediment and Greenland Ice Core Records

Here, we provide constraints on the timing and succession of major climate changes in the Northern Hemisphere connected with GI-10 (~41 ka BP) (Fig. 1). We measured a ^{10}Be record at <40-y resolution along with environmental proxy records down to subdecadal step size from Black Sea sediment core M72/5-22-GC8 (*SI Appendix*, *Supporting Information Text* and Figs. S1 and S2). All time series were measured from the same sediment core to avoid chronological uncertainties introduced through core-to-core correlation of proxy records. To isolate the ^{10}Be production rate and remove environmentally induced variability, we apply regression analysis between our ^{10}Be record and the X-ray fluorescence (XRF) derived Ca, K, Ti, and coastal ice rafted detritus (IRDc) proxies representing major environmental shifts in the Black Sea region (Black Sea and large parts of its catchment) as well as ^{10}Be/^{9}Be normalization (13, 20) (*SI Appendix*, Fig. S3). The resulting estimates of the ^{10}Be production rate (^{10}Be$_{atmosphere}$) resemble each other and the original ^{10}Be concentration record from Black Sea sediments within the studied time interval, indicating that environmental effects on ^{10}Be deposition are minor (*SI Appendix*, Fig. S3). Further indication for the preservation of the globally common cosmogenic radionuclide production signal is the multicentennial double peak in ^{10}Be, also present in the paleointensity record from Black Sea sediments around the Laschamp geomagnetic excursion (21–23) (*SI Appendix*, Fig. S3). However, since this structure is not that pronounced in the ^{10}Be flux time series from Greenland ice cores, we cannot rule out remaining uncorrected environmental influences on ^{10}Be deposition. Similarities between our ^{10}Be$_{atmosphere}$ records and ^{10}Be fluxes from the central Greenland GRIP and GISP2 ice cores on multidecadal scales could possibly point to a solar modulation of ^{10}Be production (Fig. 2). This result is supported by significant oscillations in the ^{10}Be record around 90, 160, and 210 y, likely resembling known solar activity cycles (24, 25) (*SI Appendix*, Fig. S4). However, the low significance values for the 160- and 210-y oscillations point to a slight remaining nonproduction variability in the ^{10}Be$_{atmosphere}$ records (26). The preserved multidecadal cosmogenic radionuclide production rate variations suggest a minor influence of residence times in the water column and bioturbation on our ^{10}Be record. Both effects are expected to smooth out these types of signals (27).

Our environment-corrected ^{10}Be$_{atmosphere}$ records from Black Sea sediments were synchronized to ^{10}Be fluxes from central Greenland ice cores (19) using the global optimal fit and allowing for up to 25% chronological and sampling uncertainty (28) (Fig. 2 and *SI Appendix*, *Supporting Information Text*). To test the robustness of our results and provide error ranges, the ^{10}Be$_{atmosphere}$ records were individually synchronized to the ^{10}Be flux time series from central Greenland ice cores (Fig. 2). Determined mean chronological offset between the Black Sea sediment and central Greenland ice core record on the Greenland Ice Core Chronology 2005 (GICC05)

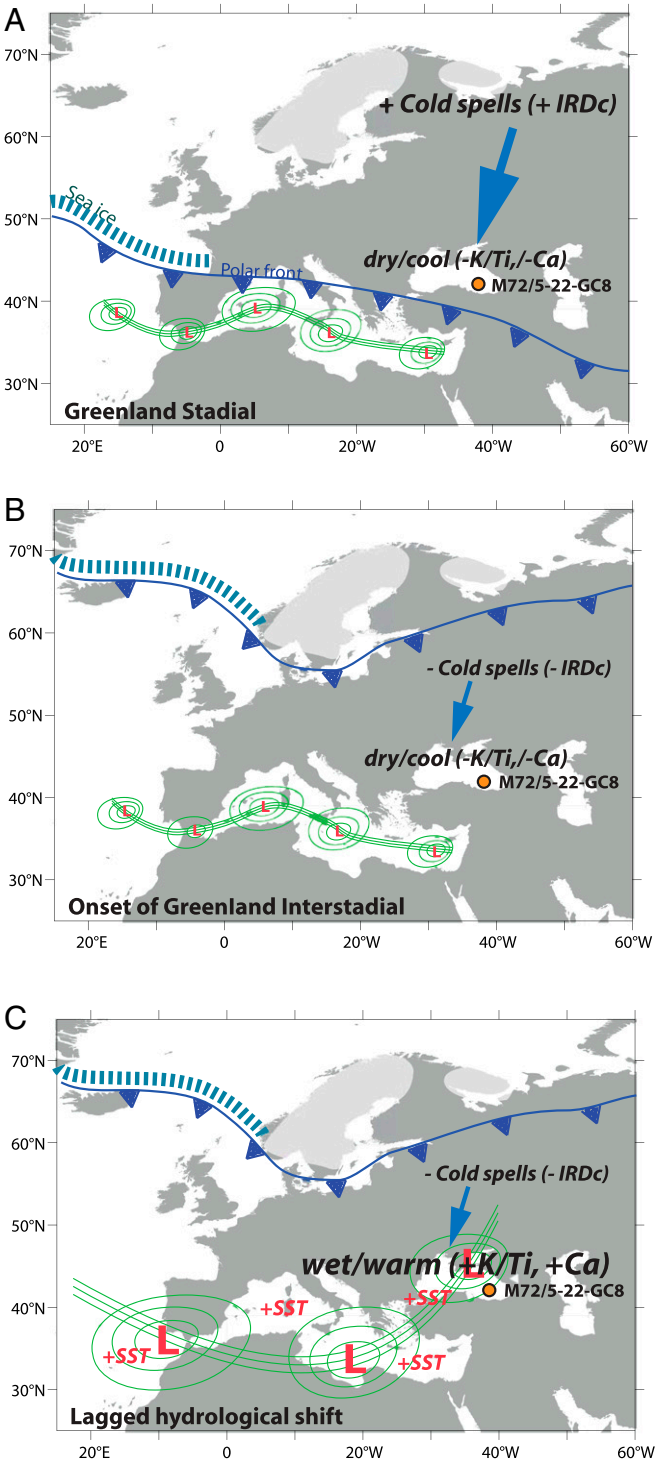

Fig. 1. Proposed succession of climate events connected with the onset of GIs in the Black Sea region. (*A*) Initial situation during Greenland stadials. (*B*) Northward shift of the polar front following sea ice retreat causing reduced cold spells in the Black Sea region at the onset of GIs. (*C*) Lagged atmospheric circulation shift at the Black Sea associated with intensified cyclonic activity after interstadial adjustment of regional thermal ocean interior. The position of Black Sea sediment core M72/5-22GC8 is highlighted. Sea ice boundaries (46) and ice sheets extents (47) are indicated.

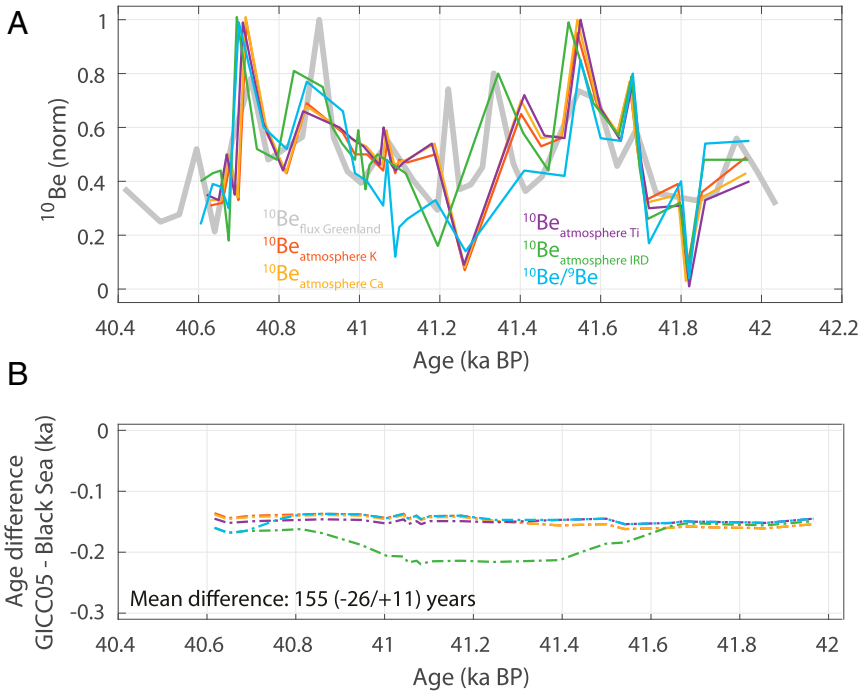

Fig. 2. Synchronized ^{10}Be records from Black Sea sediments and Greenland ice cores around GI-10 based on curve fitting. (*A*) Synchronizations of the individual environment-corrected $^{10}Be_{atmosphere}$ and $^{10}Be/^{9}Be$ records from Black Sea sediments to the ^{10}Be flux time series from the central Greenland GRIP and GISP2 ice cores on the GICC05 timescale (19) using the global optimal fit and the MATCH software (28). All records were normalized between 0 and 1. (*B*) Age difference between the Black Sea $^{10}Be_{atmosphere}$ records and ice core ^{10}Be flux. Maximum differences between the individual synchronizations are considered as synchronization error ranges. Colors in *B* correspond to those in *A*.

timescale around 41 ka BP is 155 y (−26/+11 y average uncertainty), whereby our sediment record leads the ice cores (Fig. 2). This is lower than the estimated 250-y younger age for the Greenland ice core GICC05 timescale around 41 ka BP compared to U/Th dated speleothems (19).

Delayed Climate Response in the Black Sea Region to GI-10

Corrected for the determined offset, the synchronized environmental records point to a bipartite climate response in the Black Sea region to GI-10. First, in phase with the abrupt temperature increase in Greenland, coastal sea ice decreases in the southern Black Sea during less severe winters, reflected by reduced sedimentary IRDc contents (29) (Fig. 3*A*). IRDc is composed of fine detrital grains incorporated in coastal sea ice formed along the southern Black Sea coast during severe winters with major polar cold spells (21). Subsequent ice drift and melting results in the offshore release of the material (21, 29).

Second, and with a lag of 190 (±44) y, abrupt increases in the sedimentary K/Ti ratio indicate enhanced regional precipitation causing higher riverine sediment supply into the basin (29) (Fig. 3*B*). K originates from weathering feldspars and mica and is transported into the Black Sea predominantly from the northern Danube, Dniester, and Dnieper Rivers (29). In addition, coinciding increases in Ca contents point to warmer temperatures (Fig. 3*C*). Enhanced authigenic carbonate precipitation in the Black Sea is controlled by CO_2 assimilation and pH increase through photosynthesizing phytoplankton in warmer surface waters (21, 30). A temperature-dependent carbonate precipitation during GI-9 to GI-11 is confirmed by in-phase changes between Ca and the TEX_{86} paleothermometer on the multicentennial scale (31) (*SI Appendix*, Fig. S5). Coinciding changes in arboreal pollen contents in Black Sea sediments further support the interpretation of the Ca and K/Ti ratio proxies to reflect warmer and wetter climate conditions (30) (*SI Appendix*, Fig. S5). However, the direct application of the TEX_{86} and arboreal pollen records for investigating leads and lags in the climate system connected with GIs is hampered due to their multicentennial resolution and the chronological uncertainties that would be introduced through matching data from multiple sediment cores.

To confirm the lag pattern seen in our Black Sea sediment proxies during GI-10, we measured the same set of IRDc, Ca, and K/Ti ratio data for the neighboring GI-9 and GI-11, also from sediment core M72/5-22-GC8 (Fig. 4). Supporting our results for GI-10, during both interstadials, the abrupt increases in the K/Ti ratio and Ca lag the decrease in IRDc (~50 y for GI-9 and ~200 y for GI-11) (Fig. 4). This systematic pattern provides confidence in the robustness of the detected succession of events. Furthermore, we rule out sampling artifacts as a reason for the proxy offsets, since all data were measured from the same Black Sea sediment core (*SI Appendix*, Fig. S2). A lagged in-lake response of the K/Ti ratio to one environmental forcing is also very unlikely, due to the external origin of the detrital material.

Regional Oceanic Adjustment to Interstadial Conditions

Synchronizing our high-resolution sedimentological proxy records to the δ^{18}O time series from the central Greenland NGRIP ice core on the GICC05 timescale allows us to put the succession of climate events in the continental Black Sea region connected with GI-10 in context with those from Greenland, with minimized relative chronological uncertainties (Fig. 3). The decrease in coastal sea ice on the Black Sea during less severe winters synchronous with Greenland warming at the onset of GI-10 points to an in-phase atmospheric transfer and deep inland propagation of the high-latitude temperature signal within years or decades (Fig. 3) (32). In-phase climate switches at both sites support the hypothesis of an abrupt sea ice reduction in the Nordic Seas at the onset of GIs (3, 5), causing both transfer of oceanic heat to the atmosphere and a northward displacement of

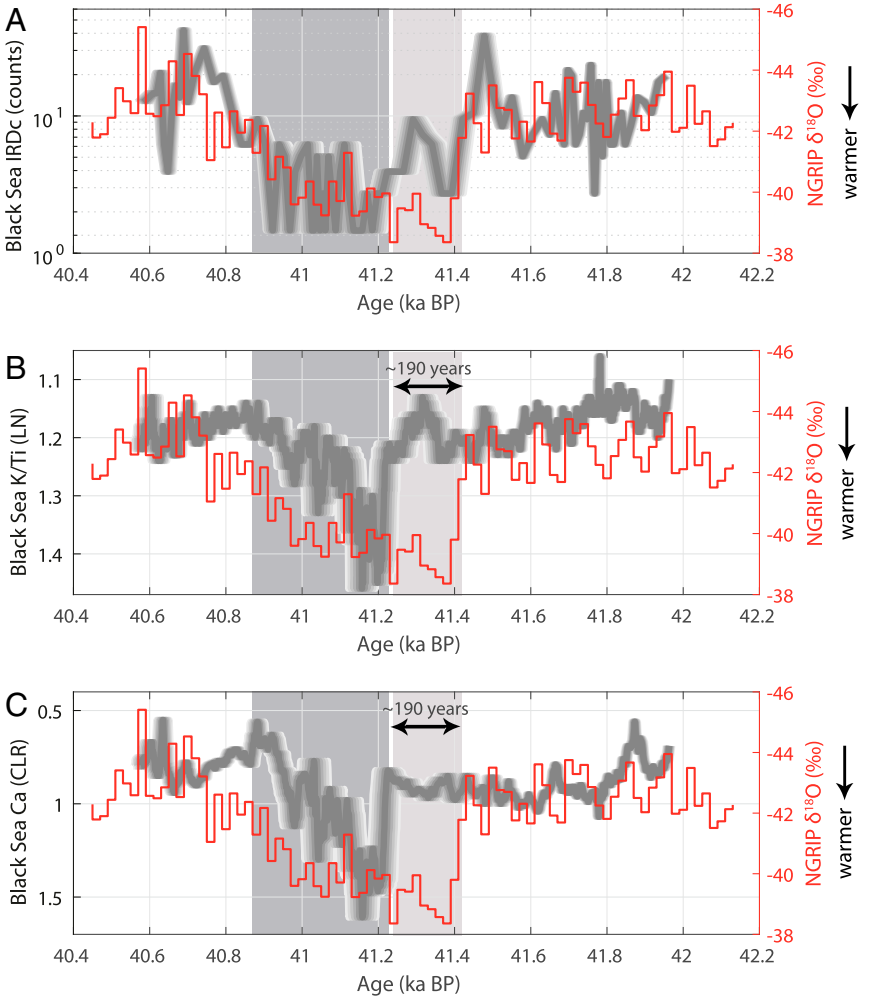

Fig. 3. Synchronized paleoclimate records from Black Sea sediment core M72/5-22GC8 and the Greenland NGRIP ice core (2) around GI-10. (*A*) Black Sea IRDc and NGRIP δ^{18}O. (*B*) Black Sea K/Ti ratio (reversed axis) and NGRIP δ^{18}O. (*C*) Black Sea Ca (reversed axis) and NGRIP δ^{18}O. The horizontal spread of the gray Black Sea graphs depicts synchronization uncertainties.

the polar front, reducing the effects of polar cold spells in the Black Sea region (Fig. 1).

This initial reduction in winter severity is followed by an increase in regional precipitation and temperature 190 (±44) y later, reflected by higher K/Ti ratios and Ca contents in the investigated Black Sea sediments (Fig. 3), best explained by a switch in the dominant mode of regional atmospheric circulation (Fig. 1). Previous studies on Black Sea sediments indicate transitions from stadials to interstadials as accompanied by switches from more continental atmospheric circulation patterns, dominated by frequent polar cold spells, to more oceanic ones characterized by intensified traversing Mediterranean cyclones, enhanced precipitation, and warmer temperatures (Fig. 1) (29). A possible cause behind the now detected lag might be a time-transgressive thermal adjustment of the regional North Atlantic, as well as Mediterranean and Black Sea interior, to the interstadial annual mean warming of ∼3 °C (31).

A comparable lag pattern of, on average, 131 y was detected between δ^{18}O and δ^{13}C in the Sofular Cave speleothem from northern Anatolia, in close proximity to the Black Sea (33). This lag was interpreted to reflect a delayed vegetation response to an initial regional climate shift associated with the onset of GIs (33). However, chronological uncertainties inhibit the investigation of phase relationships between the Sofular speleothem and Black Sea sediment record.

Our results reveal the importance of integrating high-resolution, multiproxy, and synchronized paleoclimate records for providing novel insights into the complex and time-transgressive progression of major climate shifts from the high-latitude Northern Hemisphere, which are commonly assumed to be hemispherically synchronous. They reconcile previous studies suggesting either synchronous or asynchronous climate shifts, by revealing a bipartite climate response to GI-10 in the Black Sea region, characterized by a shift in atmospheric circulation ∼190 y after an initial decrease in winter severity. We propose a time-transgressive thermal adjustment of the regional ocean (and Black Sea lake) interior as trigger of the delayed atmospheric circulation change.

Methods

Sediment Core and Initial Chronology. Sediment core M72/5-22-GC8 (42°23′N, 36°50′E) was retrieved from the Archangelsky Ridge in the southeastern Black Sea at a depth of 847 m below sea level using a gravity corer (*SI Appendix*, Fig. S1) (21). In this study, we focus on the sediment interval from 435- to 543-cm core depth covering GI-9 through GI-11. Initial chronological constraints for the SE Black Sea sediment stratigraphy were derived for the time interval 30 ka BP to 60 ka BP through tuning sedimentary IRDc and carbonate content records to δ^{18}O from the Greenland NGRIP ice core on the GICC05 timescale, all reflecting GI-like climate variability (21) (*SI Appendix*, Fig. S6). Tuning results are supported by 16 bivalve accelerator mass spectrometry (AMS) ^{14}C dates between 12.5 ka BP and 38.9 ka BP (21). The radiometrically determined ages of the Campanian Ignimbrite, 39.28 ± 0.11 ka BP (34) and

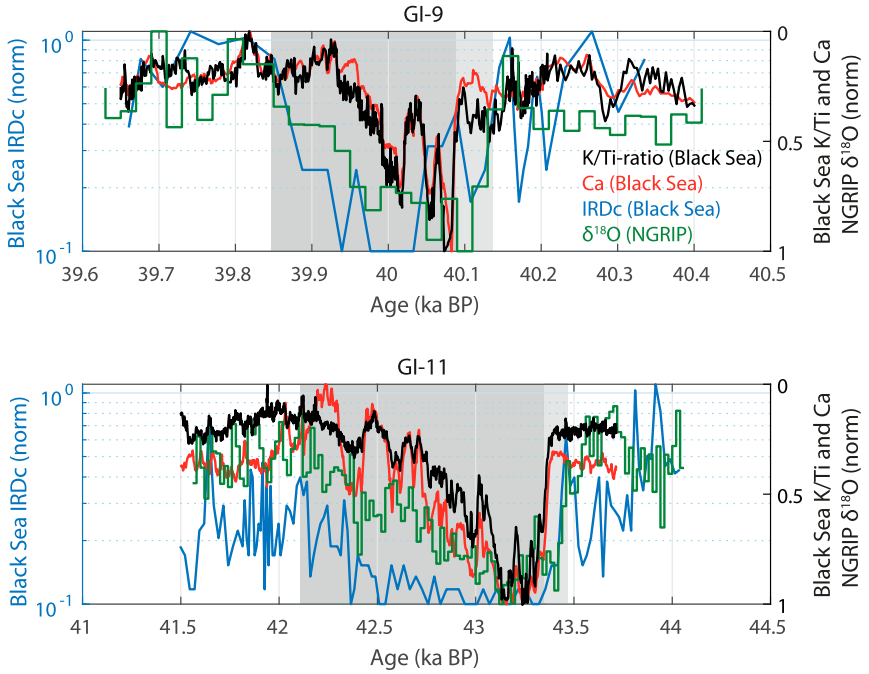

Fig. 4. Proxy responses in Black Sea sediments and the Greenland NGRIP ice core (2) during GI-9 and GI-11. Shown are IRDc as well as K/Ti ratio and Ca from Black Sea sediment core M72/5-22GC8 in comparison with $\delta^{18}O$ from the Greenland NGRIP ice core. The $\delta^{18}O$ record from the Greenland NGRIP ice core was shifted to match the IRDc time series from Black Sea sediments. Comparable to GI-10, increases in the K/Ti ratio and Ca lag the decrease in IRDc in Black Sea sediments (light gray area), and changes in $\delta^{18}O$ resemble those in IRDc (total gray area). Colors on *Bottom* correspond to those on *Top*.

39.85 ± 0.14 ka BP (35), are in broad agreement with its appearance in the Black Sea stratigraphy of a neighboring sediment core at 39.40 ka BP (21). However, due to a hiatus between 20 ka BP and 39.4 ka BP, the Campanian Ignimbrite tephra is not present in the sediment core used here, M72/5-22-GC8 (21).

Be Extractions and Measurements. For the construction of ^{10}Be and ^{9}Be records, a series of samples was collected from Black Sea sediment core M72/5-22-GC8. The central part of the Be time series around GI-10 (460- to 508-cm core depth) was continuously sampled in 1-cm steps resulting at a resolution of < 40 y. For the youngest (445- to 460-cm core depth) and oldest (508- to 540-cm core depth) parts, one 1-cm-thick sediment slice was extracted every 4 cm, resulting in a resolution of >100 y.

After the addition of 0.5 mg of ^{9}Be carrier, Be was leached from 300 mg of freeze-dried and homogenized sediment aliquots with 8 M HCl at 60 °C for 16 h (36). The undissolved sediment fraction was subsequently removed from the solutions through filtering. Addition of NH_3 and H_2SO_4 triggered the precipitation of metal hydroxides and silicates, which were again separated from the solutions by filtering. Ethylenediaminetetraacetic acid treatment led to the separation of other metals (36). Then, the samples were passed through hydrogen-form ion exchange columns in which Be was retained. Be was removed from the columns through the addition of 4 M HCl, and $Be(OH)_2$ precipitated with NH_3 at pH 10. The precipitates were washed and dehydrated three times by centrifuging and oxidized to BeO at 600 °C in a muffle furnace (13). After mixing with Nb, the samples were pressed into copper targets for AMS measurements of BeO at the Ion Beam Physics Laboratory of the Eidgenössische Technische Hochschule Zurich. Final ^{10}Be concentrations were calculated from measured $^{10}Be/^{9}Be$ ratios, normalized to the S2007N ($^{10}Be/^{9}Be = 28.1 \times 10^{-12}$) and S2010N ($^{10}Be/^{9}Be = 3.3 \times 10^{-12}$) reference standards (37).

The ^{9}Be contents were determined from the same sediment samples as used for ^{10}Be measurements by inductively coupled plasma mass spectrometry (iCAP Q, Thermo Fisher Scientific) using external calibration and Rh as internal standard to compensate matrix effects. Before the measurements, ^{9}Be was leached from the material with 10 mL of 15 vol% HCl. Precision and accuracy of ^{9}Be measurements based on acid digestions of the sediment reference material SGR-1b (US Geological Survey) were 3.6% and 5.0%, respectively. To investigate the performance of our extractions, we conducted a sensitivity test (*SI Appendix*, Fig. S7).

XRF Scanning and IRDc. Geochemical XRF measurements at 500-μm resolution were conducted on Black Sea sediment core M72/5-22-GC8 using an ITRAX core scanner at 30 kV, 55 μA, and 5 s dwell time. The device was equipped with a Cr tube and an energy-dispersive silicon drift detector (38). To reduce matrix effects and allow a linear interpretation of the data in terms of changing sediment composition, measured element counts were log-ratio transformed (39). Effects of sediment microdisturbances were circumvented using the best preserved of six parallel line scans, distributed equally across the core diameter. IRDc contents were determined from sediment core M72/5-22-GC8 at 0.5-cm resolution by counting detrital grains >150 μm from a fixed volume of 4.5-cm^3 wet-sieved sediments (21).

Estimating the Atmospheric ^{10}Be Production Signal. Two approaches were applied to isolate the ^{10}Be production signal ($^{10}Be_{atmosphere}$) and minimize nonproduction variability in our ^{10}Be concentration ($^{10}Be_{con}$) record from Black Sea sediments. First, four linear regression models were calculated between ^{10}Be concentrations and the parallel Ti, Ca, K, and IRDc time series from sediment core M72/5-22-GC8, reflecting major environmental changes in the Black Sea region (13, 21, 29). Then, the common variability was subtracted from the original $^{10}Be_{con}$ time series, to produce environment-corrected estimates of the ^{10}Be production rate ($^{10}Be_{atmosphere}$) (40).

Second, we applied $^{10}Be/^{9}Be$ normalization based on coupled Be measurements on the same sample material from Black Sea sediment core M72/5-22-GC8 (41, 42). In contrast to the atmospheric production of ^{10}Be, the stable isotope ^{9}Be originates mainly from weathering silicate rocks. However, once released into a waterbody, both isotopes are scavenged from the water column by settling particles with a similar efficiency (43). Therefore, the shared variance of sedimentary ^{10}Be and ^{9}Be concentrations is expected to reflect catchment effects, while the $^{10}Be/^{9}Be$ ratio is a proxy of the cosmogenic radionuclide production rate (41).

Timescale Synchronization. For the synchronization to the ^{10}Be flux time series from the central Greenland GRIP and GISP2 ice cores, we only use the part of the Black Sea $^{10}Be_{atmosphere}$ and $^{10}Be/^{9}Be$ records at <40-y resolution, producing acceptable <100-y synchronization error ranges. Our $^{10}Be_{atmosphere}$ estimates from Black Sea sediments were synchronized to the ^{10}Be flux record from the central Greenland GRIP and GISP2 ice cores on the GICC05 timescale through automated wiggle matching using the MATCH software (28). MATCH calculates all possible alignments between two time series to find the optimal. Therefore, the time series are divided into small segments, and an alignment score is calculated for each possible matching. This score is defined as the square of the difference between the two signals (28). Evaluating a wide

range of matches precludes the algorithm from getting trapped in a local solution. Geological realism is assured through penalty functions (28). In this study, we allow for up to 25% changes in relative sedimentation rate to account for chronological and sampling uncertainties. Synchronization error ranges are defined as the maximum differences between the five individual synchronizations.

Spectral Analysis. Spectral analysis was applied to the average of the five $^{10}Be_{atmosphere}$ realizations on the original Black Sea timescale using fast Fourier transform (44). An autoregressive model was fitted to the data, and 10,000 random versions of this model were used to estimate the spectral significance (45). Before the analysis, the $^{10}Be_{atmosphere}$ time series was detrended and equidistantly resampled to 40-y resolution.

Data Availability Statement. All study data are included in the article and *SI Appendix*.

ACKNOWLEDGMENTS. We thank the crew and captain of the R/V *Meteor* M72/5 Black Sea cruise. AMS ^{10}Be measurements were supported by an endowment of the Royal Physiographical Society of Lund (to M. Czymzik). S. Plewe is acknowledged for help with XRF measurements, H. Mück is acknowledged for extracting and counting IRDc, and A. Köhler is acknowledged for support during inductively coupled plasma mass spectrometry measurements. M. Czymzik is financed by German Research Foundation Grant CZ 227/4-1 (SyncBalt project). We are grateful to two anonymous referees whose comments helped improve the final manuscript.

1. W. Dansgaard *et al*., Evidence for general instability of past climate from a 250-kyr ice-core record. *Nature* **364**, 218–220 (1993).
2. S. O. Rasmussen *et al*., A stratigraphic framework for abrupt climatic changes during the Last Glacial period based on three synchronized Greenland ice-core records: Refining and extending the INTIMATE event stratigraphy. *Quat. Sci. Rev.* **106**, 14–28 (2014).
3. T. M. Dokken, K. H. Nisancioglu, C. Li, D. S. Battisti, C. Kissel, Dansgaard-Oeschger cycles: Interactions between ocean and sea ice intrinsic to the Nordic seas. *Paleoceanography* **28**, 491–502 (2013).
4. C. Li, A. Born, Coupled atmosphere-ice-ocean dynamics in Dansgaard-Oeschger events. *Quat. Sci. Rev.* **203**, 1–20 (2019).
5. H. Sadatzki *et al*., Sea ice variability in the southern Norwegian Sea during glacial Dansgaard-Oeschger climate cycles. *Sci. Adv.* **5**, eaau6174 (2019).
6. C. S. Lane, A. Brauer, S. P. E. Blockley, P. Dulski, Volcanic ash reveals time-transgressive abrupt climate change during the Younger Dryas. *Geology* **41**, 1251–1254 (2013).
7. J. B. Pedro *et al*., Beyond the bipolar seesaw: Toward a process understanding of interhemispheric coupling. *Quat. Sci. Rev.* **192**, 27–46 (2018).
8. I. Obreht *et al*., An annually resolved record of Western European vegetation response to Younger Dryas cooling. *Quat. Sci. Rev.* **231**, 106198 (2020).
9. H. Erlenkeuser, A. Brauer, J. Jouzel, S. J. Johnsen, U. von Grafenstein, A mid-European decadal isotope-climate record from 15,500 to 5000 years B.P. *Science* **284**, 1654–1657 (1999).
10. L. G. Henry *et al*., North Atlantic ocean circulation and abrupt climate change during the last glaciation. *Science* **353**, 470–474 (2016).
11. A. Brauer *et al*., The importance of independent chronology in integrating records of past climate change for the 60–8 ka INTIMATE time interval. *Quat. Sci. Rev.* **106**, 47–66 (2014).
12. R. Muscheler, F. Adolphi, M. F. Knudsen, Assessing the differences between the IntCal and Greenland ice-core time scales for the last 14,000 years via the common cosmogenic radionuclide variations. *Quat. Sci. Rev.* **106**, 81–87 (2014).
13. M. Czymzik *et al*., Synchronizing ^{10}Be in two varved lake sediment records to IntCal13 14C during three grand solar minima. *Clim. Past* **14**, 687–696 (2018).
14. D. Lal, B. Peters, "Cosmic ray produced radioactivity on the Earth" in *Handbuch Der Physik*, S. Flügge, Ed. (Springer, 1967), pp. 551–612.
15. S. Vogt, G. F. Herzog, R. C. Reedy, Cosmogenic nuclides in extraterrestrial materials. *Rev. Geophys.* **28**, 253–275 (1990).
16. G. M. Raisbeck *et al*., Cosmogenic ^{10}Be/^{7}Be as a probe for atmospheric transport processes. *Geophys. Res. Lett.* **8**, 1015–1018 (1981).
17. F. Adolphi, R. Muscheler, Synchronizing the Greenland ice core and radiocarbon timescales over the Holocene–Bayesian wiggle-matching of cosmogenic radionuclide records. *Clim. Past* **12**, 15–30 (2016).
18. M. Czymzik *et al*., Solar cycles and depositional processes in annual ^{10}Be from two varved lake sediment records. *Earth Planet. Sci. Lett.* **428**, 44–51 (2015).
19. F. Adolphi *et al*., Connecting the Greenland ice-core and U/Th timescales via cosmogenic radionuclides: Testing the synchroneity of Dansgaard-Oeschger events. *Clim. Past* **14**, 1755–1781 (2018).
20. Q. Simon *et al*., Increased production of cosmogenic ^{10}Be recorded in oceanic sediment sequences: Information on the age, duration, and amplitude of the geomagnetic dipole moment minimum over the Matuyama–Brunhes transition. *Earth Planet. Sci. Lett.* **489**, 191–202 (2018).
21. N. R. Nowaczyk, H. W. Arz, U. Frank, J. Kind, B. Plessen, Dynamics of the Laschamp geomagnetic excursion from Black Sea sediments. *Earth Planet. Sci. Lett.* **351–352**, 54–69 (2012).
22. J. Liu, N. R. Nowaczyk, S. Panovska, M. Korte, H. W. Arz, The Norwegian-Greenland Sea, the Laschamps, and the Mono Lake excursions recorded in a Black Sea sedimentary sequence spanning from 68.9 to 14.5 ka. *J. Geophys. Res. Solid Earth* **125**, e2019JB019225 (2020).
23. Q. Simon, N. Thouveny, D. L. Bourlès, J. Valet, Cosmogenic ^{10}Be production records reveal dynamics of geomagnetic dipole moment (GDM) over the Laschamp excursion (20–60 ka). *Earth Planet. Sci. Lett.* **550**, 116547 (2020).
24. F. Adolphi *et al*., Persistent link between solar activity and Greenland climate during the Last Glacial Maximum. *Nat. Geosci.* **7**, 662–666 (2014).
25. M. Stuiver, T. F. Braziunas, Atmospheric ^{14}C and century-scale solar oscillations. *Nature* **338**, 405–408 (1989).
26. G. M. Raisbeck *et al*., An improved north-south synchronization of ice core records around the 41 kyr ^{10}Be peak. *Clim. Past* **13**, 217–229 (2017).
27. M. Christl, Sensitivity and response of beryllium-10 in marine sediments to rapid production changes (geomagnetic events): A box model study. *Geochem. Geophys. Geosyst.* **8**, Q09015 (2007).
28. L. E. Lisiecki, P. A. Lisiecki, Application of dynamic programming to the correlation of paleoclimate records. *Paleoceanography* **17**, 1049 (2002).
29. A. Wegwerth *et al*., Northern hemisphere climate control on the environmental dynamics in the glacial Black Sea "Lake." *Quat. Sci. Rev.* **135**, 41–53 (2016).
30. L. S. Shumilovskikh *et al*., Orbital and millennial-scale environmental changes between 64 and 20 ka BP recorded in Black Sea sediments. *Clim. Past* **10**, 939–954 (2014).
31. A. Wegwerth *et al*., Black Sea temperature response to glacial millennial-scale climate variability. *Geophys. Res. Lett.* **42**, 8147–8154 (2015).
32. B. R. Markle *et al*., Global atmospheric teleconnections during Dansgaard-Oeschger events. *Nat. Geosci.* **10**, 36–40 (2017).
33. D. Fleitmann *et al*., Timing and climatic impact of Greenland interstadials recorded in stalagmites from northern Turkey. *Geophys. Res. Lett.* **36**, L19707 (2009).
34. B. De Vivo *et al*., New constraints on the pyroclastic eruptive history of the Campanian volcanic Plain (Italy). *Mineral. Petrol.* **73**, 47–65 (2001).
35. B. Giaccio, I. Hajdas, R. Isaia, A. Deino, S. Nomade, High-precision ^{14}C and ^{40}Ar/^{39}Ar dating of the Campanian Ignimbrite (Y-5) reconciles the time-scales of climatic-cultural processes at 40 ka. *Sci. Rep.* **7**, 45940 (2017).
36. A. M. Berggren, A. Aldahan, G. Possnert, E. Haltia-Hovi, T. Saarinen, ^{10}Be and solar activity cycles in varved lake sediments, AD 1900-2006. *J. Paleolimnol.* **44**, 559–569 (2010).
37. M. Christl *et al*., The ETH Zurich AMS facilities: Performance parameters and reference materials. *Nucl. Instrum. Methods Phys. Res. Sect. B Beam Interact. Mater. At.* **294**, 29–38 (2013).
38. I. W. Croudace, L. Löwemark, R. Tjallingii, B. Zolitschka, Current perspectives on the capabilities of high resolution XRF core scanners. *Quat. Int.* **514**, 5–15 (2019).
39. G. J. Weltje, R. Tjallingii, Calibration of XRF core scanners for quantitative geochemical logging of sediment cores: Theory and application. *Earth Planet. Sci. Lett.* **274**, 423–438 (2008).
40. M. Czymzik *et al*., A varved lake sediment record of the ^{10}Be solar activity proxy for the Lateglacial-Holocene transition. *Quat. Sci. Rev.* **153**, 31–39 (2016).
41. Q. Simon *et al*., Authigenic ^{10}Be/^{9}Be ratio signature of the Matuyama–Brunhes boundary in the Montalbano Jonico marine succession. *Earth Planet. Sci. Lett.* **460**, 255–267 (2016).
42. L. Ménabréaz, D. L. Bourlès, N. Thouveny, Amplitude and timing of the Laschamp geomagnetic dipole low from the global atmospheric ^{10}Be overproduction: Contribution of authigenic ^{10}Be/^{9}Be ratios in west equatorial Pacific sediments. *J. Geophys. Res.* **117**, B11101 (2012).
43. F. von Blanckenburg, J. Bouchez, H. Wittmann, Earth surface erosion and weathering from the ^{10}Be (meteoric)/^{9}Be ratio. *Earth Planet. Sci. Lett.* **351-352**, 295–305 (2012).
44. M. Ghil *et al*., Advanced spectral methods for climatic time series. *Rev. Geophys.* **40**, 1003–1043 (2002).
45. L. Sha *et al*., Solar forcing as an important trigger for West Greenland sea-ice variability over the last millennium. *Quat. Sci. Rev.* **131**, 148–156 (2016).
46. C. Li, D. S. Battisti, C. M. Bitz, Can North Atlantic sea ice anomalies account for Dansgaard-Oeschger climate signals? *J. Clim.* **23**, 5457–5475 (2010).
47. C. L. Batchelor *et al*., The configuration of Northern Hemisphere ice sheets through the Quaternary. *Nat. Commun.* **10**, 3713 (2019).